JBIC (2000) 5:110–118

ORIGINAL ARTICLE

**Stefano Benini · Wojciech R. Rypniewski
Keith S. Wilson · Silvia Miletti · Stefano Ciurli
Stefano Mangani**

The complex of *Bacillus pasteurii* urease with acetohydroxamate anion from X-ray data at 1.55 Å resolution

Received: 21 July 1999 / Accepted: 15 November 1999

Abstract The structure of *Bacillus pasteurii* urease inhibited with acetohydroxamic acid was solved and refined anisotropically using synchrotron X-ray cryogenic diffraction data (1.55 Å resolution, 99.5% completeness, data redundancy = 26, *R*-factor = 15.1%, PDB code 4UBP). The two Ni ions in the active site are separated by a distance of 3.53 Å. The structure clearly shows the binding mode of the inhibitor anion, symmetrically bridging the two Ni ions in the active site through the hydroxamate oxygen and chelating one Ni ion through the carbonyl oxygen. The flexible flap flanking the active site cavity is in the open conformation. The possible implications of the results on structure-based molecular design of new urease inhibitors are discussed.

Key words Urease · *Bacillus pasteurii* · X-ray diffraction · Nickel · Acetohydroxamic acid

Abbreviations *AHA*: acetohydroxamic acid · *BME*: β-mercaptoethanol · *BPU*: *Bacillus pasteurii* urease · *DAP*: diamidophosphate · *KAU*: *Klebsiella aerogenes* urease · *PPD*: phenyl phosphorodiamidate

S. Benini · W.R. Rypniewski
EMBL c/o DESY, Notkestrasse 85, D-22603 Hamburg
Germany

K.S. Wilson
Department of Chemistry, University of York, Heslington
York, YO1 5DD, UK

S. Miletti · S. Ciurli (✉)
Institute of Agricultural Chemistry, University of Bologna
Viale Berti Pichat 10, I-40127 Bologna, Italy
e-mail: sciurli@agrsci.unibo.it
Fax: +39-051-243362

S. Mangani (✉)
Department of Chemistry, University of Siena
Pian dei Mantellini 44, I-53100 Siena, Italy
e-mail: mangani@unisi.it
Fax: +39-0577-280405

Introduction

The abrupt increase of pH, caused by the rapid hydrolysis of urea catalyzed by the Ni-containing enzyme urease (urea amidohydrolase, E.C. 3.5.1.5), is the major cause of the negative side-effects of urease activity both on human and animal health [1–3] and in agriculture [1, 4, 5]. The use of urease inhibitors has been proposed to counteract these drawbacks, but their efficiency is low, and they result in major side effects in humans [1, 3, 6, 7] and cause problems in the environment [1, 8]. Rational, structure-based molecular design of new and efficient urease inhibitors requires detailed information on the enzyme active site and catalytic mechanism [9].

The structures of *Bacillus pasteurii* urease (BPU), both in the native form [10] and inhibited with phenyl phosphorodiamidate (PPD) [10] and β-mercaptoethanol (BME) [11], have recently been reported. In native BPU (PDB code 2UBP) the two Ni ions are bridged by the carboxylate group of the carbamylated $Lys^{\alpha 220*}$, bound to Ni(1) through Oθ1 and to Ni(2) through Oθ2. Ni(1) is further coordinated by $His^{\alpha 249}$ Nδ and $His^{\alpha 275}$ N , while Ni(2) is bound to $His^{\alpha 137}$ N , $His^{\alpha 139}$ N , and $Asp^{\alpha 363}$ Oδ1 (Fig. 1A). The Ni-Ni distance is 3.7 Å. The coordination geometry is pseudo square pyramidal for the pentacoordinated Ni(1) and pseudo octahedral for the hexacoordinated Ni(2), consistent with extended X-ray absorption fine structure (EXAFS) data on native BPU [12]. Four well-ordered water/hydroxide molecules constitute a tetrahedral cluster in the vicinity of the Ni ions: one of these (W_B) symmetrically bridges the two Ni ions, and was suggested to be in the hydroxo form, while two water molecules, W_1 and W_2, complete the coordination polyhedron around the Ni ions. The fourth water (W_3) is bound to the first three solvent molecules by H-bonds, and is not involved in any coordination bonds with the Ni ions [9, 10].

In crystals of BPU obtained from solutions containing the slow, tight-binding inhibitor PPD (PDB code 3UBP), a molecule of diamidophosphoric acid (DAP),

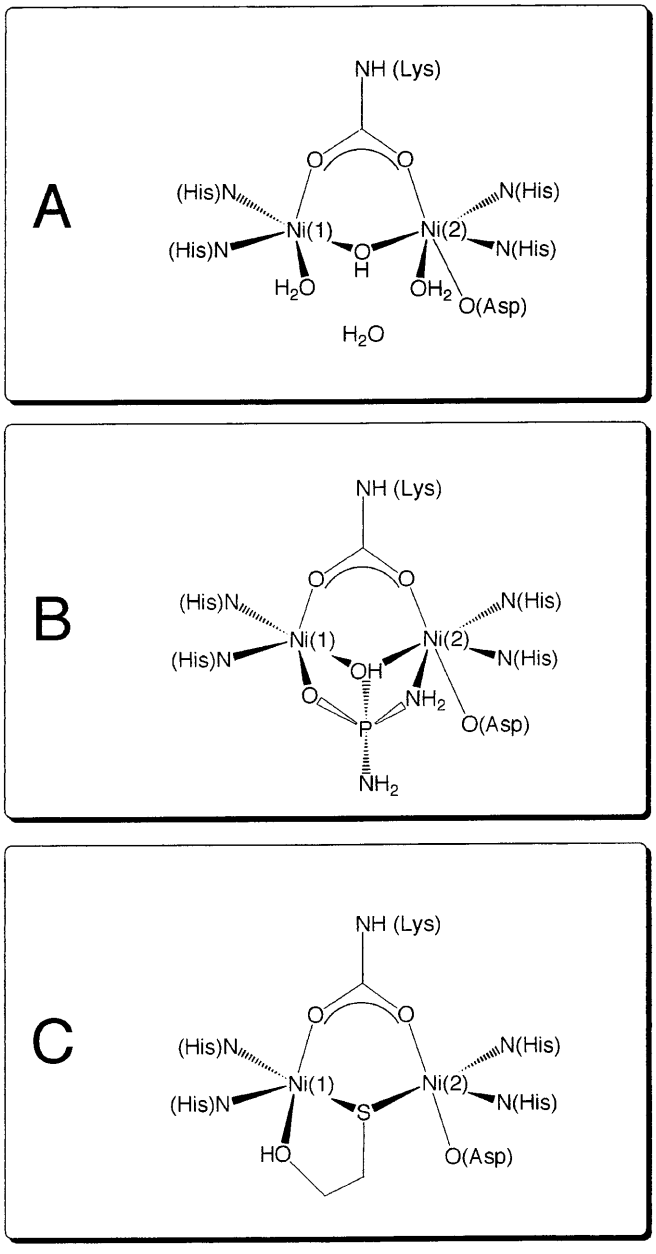

Fig. 1 Schemes for the active site Ni coordination of **A** native, **B** DAP-inhibited, and **C** BME-inhibited BPU

the product of the enzymatic hydrolysis of PPD [13], is coordinated to Ni(1) and to Ni(2) using three of the four atoms potentially available for coordination (Fig. 1B): one oxygen atom, identified as an OH group, bridges the two Ni ions, while one oxygen and one nitrogen atom bind to Ni(1) and Ni(2), respectively. The second nitrogen atom points away towards the cavity opening [9, 10]. The Ni-Ni distance is 3.8 Å. The tetrahedral DAP exactly replaces the cluster of solvent molecules found in native BPU, and its binding does not change the coordination geometry of the Ni ions with respect to the native enzyme. This latter observation is consistent with EXAFS studies reported for PPD-inhibited BPU [12].

DAP is a transition state analogue, and its mode of binding to the Ni ions, together with a comparison between native and DAP-inhibited urease structures, prompted us to propose a novel mechanism for enzymatic urea hydrolysis, which reconciled the available structural and biochemical data [9, 10]. This mechanism involves a direct role of both Ni ions in binding and activating the substrate, and of the Ni bridging hydroxide as the nucleophile in the process of urea hydrolysis. Comparison of the structures of native and DAP-inhibited BPU reveals two distinct conformations of the flap lining the active site cavity, and suggests a role for this motif in stabilizing the catalytic transition state and accelerating the reaction [9, 10].

In BPU inhibited with BME (PDB code 1UBP) the sulfur atom of BME symmetrically bridges the binuclear Ni center, with a Ni-Ni distance of 3.1 Å. BME further chelates Ni(1) using its terminal OH [9, 11] (Fig. 1C), resulting in both Ni ions being pentacoordinated.

Urease inhibition by hydroxamic acid derivatives, first shown to occur as early as 1962 [14], has been studied on enzymes isolated from plants (jack bean [15, 16]), from bacteria (reviewed in [1, 3]), and from soil [17]. Electron spectroscopy [16] and magnetism [18] studies indicated that inhibitors of this class bind to the Ni ions in the active site. The most studied of such derivatives is acetohydroxamic acid (AHA, Scheme 1), shown to behave as a slow binding (hours) competitive inhibitor [15, 16, 19].

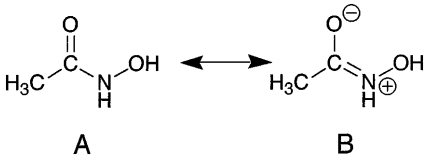

Scheme 1

The room temperature structure of a recombinant mutant form of *Klebsiella aerogenes* urease (KAU) complexed with AHA has been reported (PDB code 1FWE) [20]. The inhibitor was shown to bridge and chelate the Ni ions with the amidohydroxyl and the carbonyl groups of the inhibitor, respectively, with a pronounced asymmetry for the Ni-bridging atom [Ni(1)-O_B = 2.6 Å; Ni(2)-O_B = 1.8 Å].

The present report provides new and detailed structural information on the mode of BPU inhibition with AHA, integrating the results reported for KAU, and providing further insights that are potentially useful for structure-based rational design of urease-related drugs. Furthermore, a comparative analysis of the amino acid sidechains involved in Ni binding, among all structures available so far, reveals possible movements crucial for the enzymatic hydrolysis and support our recently proposed urease mechanism [9, 10].

Materials and methods

Protein isolation and crystallization

BPU was isolated and purified to a specific activity of ca. 2500 units/mg as previously reported [21]. Crystallization of AHA-inhibited urease was achieved at 20 °C using the hanging drop method. A solution containing 11 mg/mL of urease in 50 mM sodium phosphate at pH 7.5, containing 50 mM Na_2SO_3, was exchanged with a solution of 20 mM Tris-HCl (pH 8.0) containing 4 mM AHA. The resulting solution (3 μL) was diluted with 3 μL of precipitant (a saturated ammonium sulfate solution containing 1.2 M LiCl, diluted to 50% with 100 mM sodium citrate, pH 6.3, and 4 mM AHA), and equilibrated against 500 μL of precipitant. Rice-shaped single crystals, of about 0.4 × 0.4 × 0.7 mm on average, formed in few days.

Data collection and evaluation

Diffraction data were collected on a single crystal of the AHA-inhibited BPU at 100 K using synchrotron radiation from the BW7B wiggler line of the DORIS storage ring at the EMBL outstation at DESY, Hamburg (Germany). The detector was a 30-cm MarResearch imaging plate scanner. For cryoprotection, a single crystal of AHA-inhibited BPU, of dimensions 0.3 × 0.3 × 0.5 mm, was transferred from the crystallization drop into 500 μL of the precipitant solution. The concentration of the cryoprotectant was gradually increased from 0 to 15% by adding 100 μL portions of 20% ethylene glycol, at 1 min intervals. The crystal was transferred to a solution containing 20% ethylene glycol, scooped up in a cryo-loop, and rapidly exposed to a cold nitrogen stream.

The data were processed using the program DENZO and merged with SCALEPACK [22]. Table 1 reports a summary of data statistics for AHA-inhibited BPU. The high-resolution limit was chosen by keeping reflections in the highest resolution bin if at least 50% had $I/\sigma>2$ [23]. The cell is almost isomorphous with that of the native enzyme (Table 1) and contains four urease molecules lying in the special positions of point symmetry 3. Therefore the asymmetric unit consists of one third (one $\alpha\beta\gamma$ moiety [10]) of the urease molecule.

Table 1 X-ray data collection statistics and data reduction for AHA-inhibited BPU

Wavelength (Å)	0.8342
Resolution range (Å)	32.50–1.55
R_{merge} [a]	0.071
Raw measurements	3,612,270
Unique reflections	138,830
Redundancy	26.02
% completeness	99.5
% completeness [high-resolution bin (Å)]	99.5 (1.58–1.55)
% Greater than 3σ	65
I/σ in high-resolution bin	2.2
Space group	$P6_322$
$a=b$ (Å)	130.88
c (Å)	189.00

[a] $R_{merge} = \sum |I_i - <I>| / \sum <I>$, where I_i is an individual intensity measurement and $<I>$ is the average intensity for this reflection with summation over all the data

Structure determination and refinement

Initial phases for AHA-inhibited BPU were obtained from the refined model of the native enzyme (PDB code 2UBP [10]), from which the active site residues, the metal ions, the sulfate anion, the flexible loop region, and all water molecules were omitted. The protein regions displaying different conformations were manually rebuilt with the program O [24]. The structure of AHA-inhibited BPU was refined using REFMAC cycles [25] with established geometric targets [26]. Randomly selected reflections (2% of the total) were used as an R_{free} set for cross validation. No restraints were used for the Ni-ligand distances. Automatic solvent building was performed using the program ARP, keeping only those water molecules having density greater than 1.5σ in the $2F_o–F_c$ electron density map [27]. Omit maps were calculated after several refinement cycles of a model from which the AHA atoms were excluded. Using isotropic temperature factors the refinement converged to R and R_{free} of 18.8 and 21.2, respectively. At this point the high redundancy of the data allowed us to perform an anisotropic refinement of the structure with anisotropic temperature factors for each atom in the model using REFMAC [28], in order to improve R and R_{free} as well as the fit to geometric targets. The stereochemistry of the final model was checked using the programs WHATIF [29] and PROCHECK [30]. Table 2 reports a summary of the crystallographic analysis and refinement. The refined crystallographic coordinates for AHA-inhibited BPU have been deposited in the Brookhaven Data Bank under the accession code 4UBP.

Table 2 Summary of the crystallographic analysis and refinement for AHA-inhibited BPU

Protein atoms	6056
Solvent atoms	746
Bound metal ions	2 Ni
Bound AHA atoms	5
Temperature factors for protein atoms (Å^2)	24.38
Temperature factors for solvent (Å^2)	41.01
Temperature factors for Ni(1), Ni(2) (Å^2)	22.15, 20.54
Average temperature factors for AHA atoms (Å^2)	26.51
R.m.s. bond length deviation (Å)	0.013
R.m.s. bond angle deviation (Å)	0.030
R.m.s. planes deviation (Å)	0.038
R.m.s. on atomic positions from σA plots (Å)	0.063
R.m.s. on final $2F_o–F_c$ electron density map (electrons/Å^3)	0.35
Ramachandran most favored region (%)	90.1
Ramachandran additional allowed region (%)	8.7
Ramachandran generously allowed region (%)	1.1
R-factor (R-free) [a] (%)	15.1 (19.0)

[a] $R\text{-factor} = \sum ||F_o| - |F_c|| / \sum |F_o|$; R-factor and R-free are calculated by using the working and free reflection sets, respectively; the free reflections (2% of the total) were held aside throughout the refinement

Results

Overall structure of AHA-inhibited BPU

The AHA-inhibited BPU structure closely matches that of native BPU with an overall r.m.s.d. of only 0.156 Å between the two structures, based on superposition of the complete set of Cα atoms of the three subunits. Therefore, the binding of AHA does not affect the $\alpha_3\beta_3\gamma_3$ quaternary structure of BPU. The residue-averaged B-factors of the crystallographically equivalent α-, β-, and γ-subunits for native BPU, and BPU inhibited with DAP, BME, and AHA, are shown in Fig. 2. It is evident from this figure that the residues in the ranges 315–336 and 388–398 in the α-subunit of all these structures have average B-factors 3–5 times high-

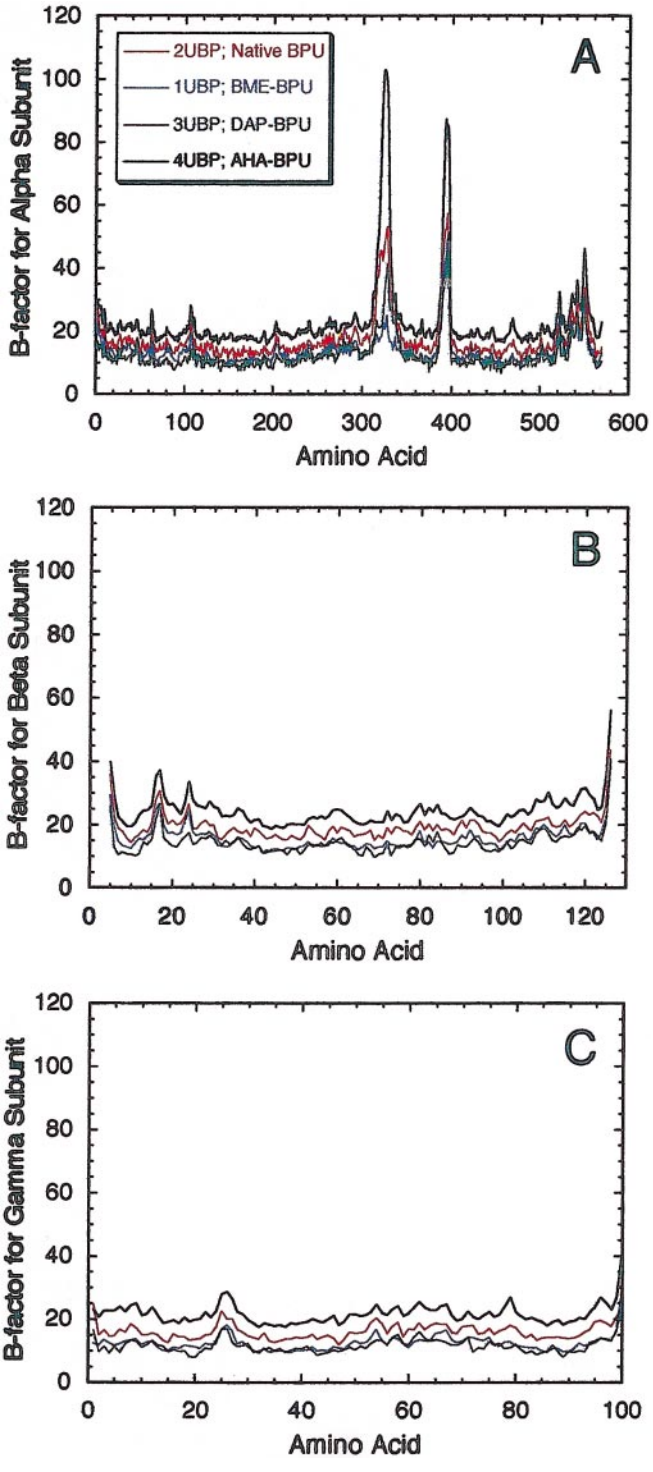

Fig. 2 Residue-averaged main chain *B*-factors for the three chains (**A** α subunit, **B** β subunit, **C** γ subunit) of native (2UPB), BME (1UPB), DAP (3UPB), and AHA (4UPB) inhibited BPU

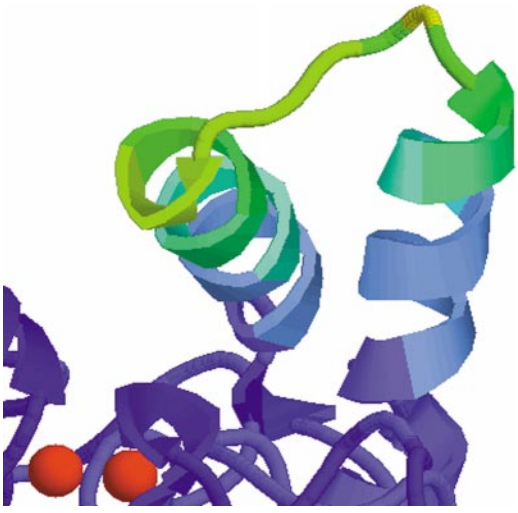

Fig. 3 Ribbon diagram of the active site loop region in AHA-inhibited BPU, colored according to the *B*-factors (from blue to red the *B*-factors increase). The Ni ions are shown as *red spheres*

er than in the other residues of the subunit. However, the electron density from $2F_o$–F_c maps at the 0.5σ level is sufficiently clear to allow us to build a model for the loops. The 315–336 region is part of the flexible helix-loop-helix motif constituting the flap cover of the active site cavity [9–11, 31]. This flap has been proposed to act as a gate for the entrance of the substrate to the active site [10, 31], but could also take part in the assembly of the dinickel center from apo-urease [9]. In this region the average *B*-factor for AHA-inhibited BPU is 64.3 Å^2. Figure 3 shows a ribbon drawing of the active site loop region in AHA-inhibited BPU, color-coded according to the average *B*-factors of each residue. The second region of high mobility (average *B*-factor 72.8 Å^2) consists of residues 388–398, which constitute the loop linking the last helix of the $(\alpha b)_8$ barrel (helix 8) with a helix (H5) not belonging to the barrel motif (the secondary structure nomenclature follows [32]), and is far from the active site. The flexible flap in AHA-inhibited BPU mainly adopts the "open" conformation, as observed in native BPU [10]. The lower mobility in native BPU (see Fig. 2) can be attributed to the presence of a sulfate ion bound in the cavity, linking Arg$^{\alpha 339}$ to the flap residue His$^{\alpha 323}$ through strong charge-assisted H-bonds, which stabilize the flap in the open conformation [10]. In the present structure a similar adduct is not present despite the fact that the crystals were obtained from the same sulfate-rich crystallization solution. Among all BPU structures so far available, the BME-bound complex possesses the most ordered flap (see Fig. 2), again in the "open" conformation [11]. This is explained by the presence of a second molecule of BME, forming a mixed disulfide bond with the flap residue Cys$^{\alpha 322}$ and involved in an H-bond between its α-hydroxyl group and the carbonyl oxygen atom of the inner residue Ala$^{\alpha 366}$, positioned on a neighboring loop. The flexibility of the flap is thereby reduced, and the entrance to the active site is sealed by steric hindrance. Finally, a "closed" flap is found in DAP-inhibited BPU, where two H-bonds between the

distal NH_2 group of the Ni-bound inhibitor, and $His^{\alpha323}$ and $Ala^{\alpha366}$, stabilize this conformation [10].

The active site structure of AHA-inhibited BPU

The electron density from a $2F_o–F_c$ difference map contoured at 1.0σ, superimposed on the refined atomic model of the active site of the complex, is shown in Fig. 4A. The final omit map contoured at 4.0σ, showing the inhibitor electron density, is reported in Fig. 4B. One AHA molecule is complexed to the Ni ions in the active site, while no other inhibitor molecules are present either in the cavity or in any other part of the urease structure. Figure 5A shows the refined atomic model of AHA bound to the dinickel center. The arrangement of the protein ligands bound to the Ni ions in the AHA-BPU adduct is essentially identical to that in native BPU [10] (see Fig. 5B) and Table 3 compares relevant distances observed in the active sites of all available BPU structures.

Both Ni ions are well ordered [*B*-factors of 22.1 and 20.5 $Å^2$ for Ni(1) and Ni(2), respectively] and five-coordinated. The structural index parameter

$$\tau = \frac{(\beta - \alpha)}{60} \quad (1)$$

introduced by Addison et al. [33] can be used to better define the geometry around five-coordinate metal ions (see Scheme 2): according to this criterion, α and β ($\beta \geq \alpha$) are the two largest angles around the central atom, so that $\tau = 1$ for perfectly trigonal bipyramidal (TB) geometry whereas $\tau = 0$ for square pyramidal (SPY) geometry. For five-coordinate structures, the index τ can be used to describe the structural continuum between ideal SPY and TB geometries.

In the case of AHA-inhibited BPU, the value of $\tau = 0.363$ for Ni(1) can be compared with those obtained from the structures of DAP-inhibited BPU ($\tau = 0.067$), native BPU ($\tau = 0.157$), and BME-inhibited BPU ($\tau = 0.223$), indicating a marked increase of the TB character. The value of $\tau = 0.365$ for Ni(2) in AHA-BPU can be compared with that obtained from the structure of BME-inhibited BPU ($\tau = 0.443$) [in native and DAP-BPU the Ni(2) ion is hexacoordinate], indicating a smaller TB character in AHA-BPU. As a general consideration, the values of the parameter τ for all the coordination geometries of the Ni(1) ion in the active site of the four BPU derivatives so far characterized indicate a preference for five-coordinate SPY geometry with various degrees of distorsion towards a TB arrangement. On the other hand, Ni(2) could be penta- or hexacoordinate: in the former case the geometry is predominantly SPY, slightly distorted towards TB, while in the latter case the geometry is distorted octahedral.

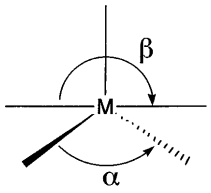

Scheme 2

The binding of AHA to the active site of BPU provides a bridge between Ni(1) and Ni(2) through the hydroxamate oxygen (O_B), in addition to the ubiquitous presence of the bridging carbamate group of the post-transcriptionally modified $Lys^{\alpha220*}$. The hydroxamate O_B atom of AHA replaces the bridging hydroxide molecule (W_B) present in the structure of native BPU [10], and the resulting bridge is symmetric (Ni-O_B = 2.0 Å). The binding of AHA causes shortening of the Ni(1)-Ni(2) distance by about 0.2 Å with respect to the native enzyme (see Table 3). This effect, although significant, is far less pronounced than that in the BME-inhibited enzyme, for which a decrease of 0.6 Å was observed [11].

The second AHA oxygen (O_T) is bound to Ni(1), completing a chelating binding mode of the inhibitor. The coordination of O_T to N(1) is assisted by an H-bond donated by the $His^{\alpha222}$ N proton; this arrangement is analogous to that in the native enzyme around

Table 3 Relevant distances (Å) in the active site of native and inhibited ureases (BPU consensus sequence numbering)

Protein PDB codes	Native UBP 2UBP	DAP-BPU 3UBP	BME-BPU 1UBP	AHA-BPU 4UBP	AHA-KAU 1FWE
Ni(1)-Ni(2)	3.7	3.8	3.1	3.5	3.7
$His^{\alpha249}$ Nδ-Ni(1)	2.2	2.0	2.2	2.0	2.2
$His^{\alpha275}$ N -Ni(1)	2.2	2.1	2.2	2.0	2.3
$Lys^{\alpha220*}$ Oθ1-Ni(1)	2.1	2.1	2.1	2.0	2.1
AHA O_B(W_B, S_B)-Ni(1)	2.1	2.3	2.3	2.0	2.6
AHA O_T(W_1)-Ni(1)	2.2	2.2	2.3	2.2	2.0
$His^{\alpha137}$ N -Ni(2)	2.2	2.1	2.1	2.0	2.3
$His^{\alpha139}$ N -Ni(2)	2.2	2.2	2.1	2.0	2.2
$Lys^{\alpha220*}$ Oθ2-Ni(2)	2.1	1.9	2.1	2.0	2.1
$Asp^{\alpha363}$ Oδ1-Ni(2)	2.2	2.1	2.1	2.1	2.2
AHA O_B(W_B, S_B)-Ni(2)	2.2	2.3	2.3	2.0	1.8

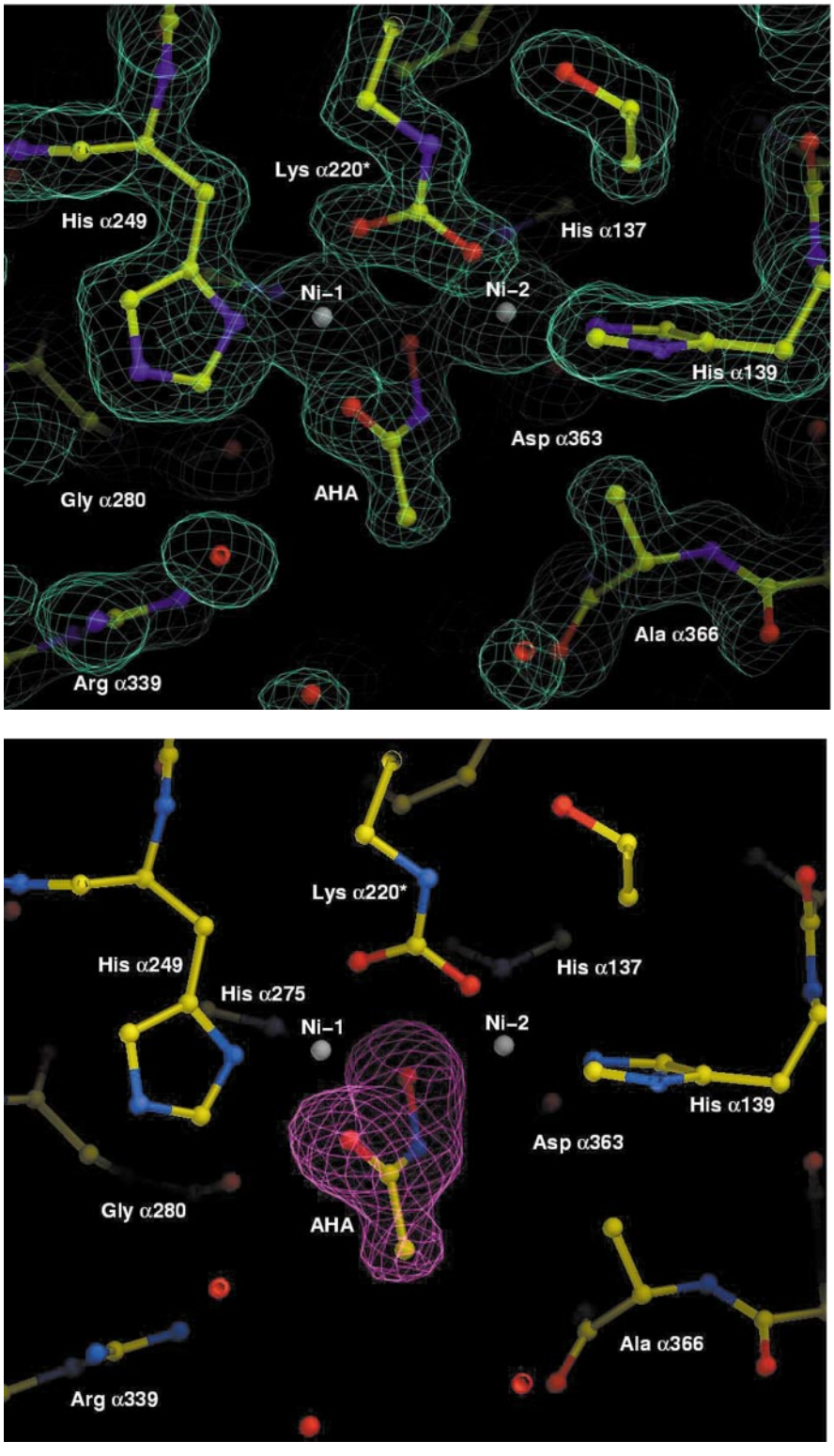

Fig. 4 **A** Atomic model of the active site of AHA-inhibited BPU, showing the Ni coordination environment superimposed on the final $2F_o–F_c$ electron density map contoured at 1.0σ. **B** Omit map of the AHA molecule calculated with Fourier coefficients $F_o–F_c$ and phases derived from the final model from which the AHA atoms had been removed (purple map, contoured at 4.0σ)

the water molecule (W_1) bound to Ni(1) [10], the only difference being that in the present structure this H-bond is ca. 0.2 Å shorter (2.73 Å). The AHA O_T atom is in van der Waals contact with the $Ala^{\alpha 170}$ O atom (3.3 Å) and a water molecule (W_{379}, 3.4 Å) in the active site cavity, but the configurations of these contacts indicate that they are not H-bonds. The binding of AHA displaces all four water/hydroxyde molecules crystallographically detected in the active site of native BPU.

The $Asp^{\alpha 363}$ carboxylate group is rotated about the Cβ-Cγ bond by 35° with respect to its conformation in native BPU to receive an H-bond from the AHA-NH

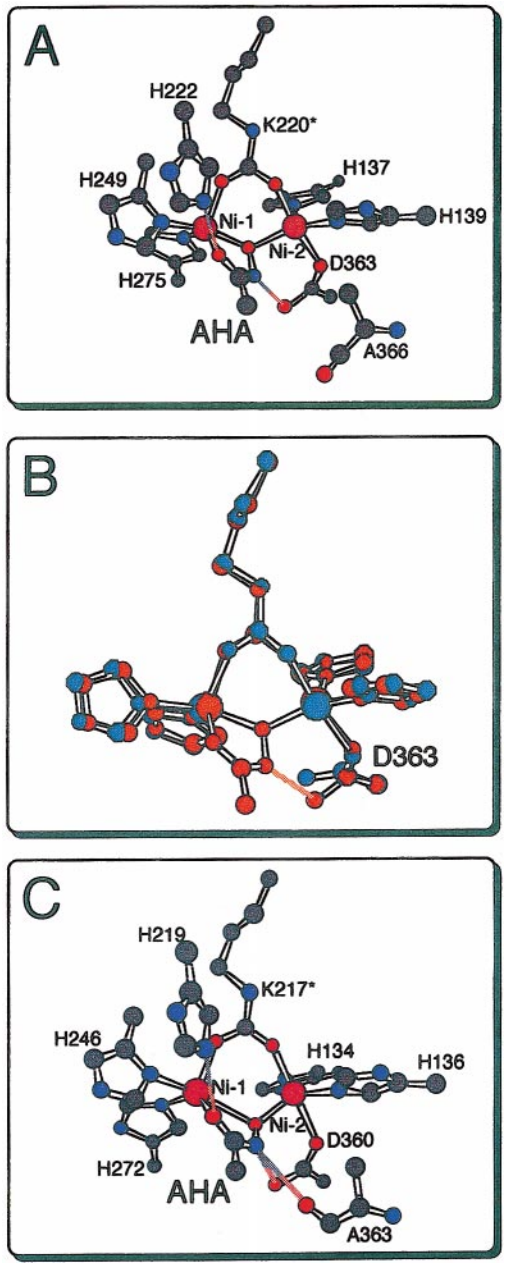

Fig. 5 **A** Refined model of the active site structure of AHA-inhibited BPU. The two Ni ions are shown as *purple spheres*. Hydrogen bonds are colored according to the donor-acceptor CPK color code. **B** Least-squares fit of the metal-bound active site residues in native (*orange*) and AHA-inhibited BPU (*blue*). **C** Refined model of the active site structure of AHA-inhibited KAU colored as in **A**

group (AHA NH-Asp$^{\alpha 363}$ Oδ2 = 2.6 Å), further stabilizing the inhibitor binding (Fig. 5B). The consequence of this movement is an increase of the Asp$^{\alpha 363}$ Oδ2-O$_B$ distance (3.0 Å) with respect to the corresponding Asp$^{\alpha 363}$ Oδ2-W$_B$ distance in native BPU (2.5 Å), suggesting the presence of repulsive electrostatic interactions between O$_B$ and Asp$^{\alpha 363}$ Oδ2. This observation suggests that O$_B$ is deprotonated and that AHA binds in the anionic hydroxamate form.

Among the conserved amino acid residues not involved in Ni binding but thought to be important in the catalytic mechanism (Ala$^{\alpha 170}$, His$^{\alpha 222}$, Glu$^{\alpha 223}$, Asp$^{\alpha 224}$, Gly$^{\alpha 280}$, Cys$^{\alpha 2\ 322}$, His$^{\alpha 323}$, Ala$^{\alpha 366}$, Met$^{\alpha 367}$) [10, 31], only Met$^{\alpha 367}$ has a different conformation with respect to native BPU, with its sidechain methyl group pointing in the opposite direction.

Discussion

The X-ray structure of AHA-inhibited BPU reveals that inhibition occurs by direct binding of the inhibitor to the Ni ions in the active site. As already observed for the BME-BPU complex [11], the AHA molecule behaves as a bridging-chelating ligand. These two structures reveal a common feature of this dinuclear active site: the more negatively charged donor atom of the inhibitor bridges the two Ni ions; if a second donor is available, it will bind to Ni(1), which has an unsaturated coordination sphere and therefore is the metal site with the highest positive charge density. Another general aspect which is revealed by the inhibitor binding studies on BPU is that the Ni(2)-bound Asp$^{\alpha 363}$ sidechain is able to adopt different conformations in order to optimize the inhibitor binding through an H-bond involving its Oδ2 atom. Indeed, this residue's carboxylate group can assist and stabilize both a bridging OH group in native and DAP-inhibited BPU [9, 10] and the AHA NH group in the present structure, by changing its sidechain conformation while still maintaining its coordination to Ni(2). The direct observation of such conformational flexibility of Asp$^{\alpha 363}$ further supports our recently proposed mechanism for urease, which involves a proton transfer from the Ni-bridging OH group to the distal NH_2 group of urea through Asp$^{\alpha 363}$ Oδ2, a residue which is supposed to be able to adopt different conformations in order to carry out such a function [9, 10].

The presence of a well-ordered water molecule (W$_{99}$, $B = 25.4$ Å^2) in the AHA- and BME-inhibited urease at the same position where a sulfate ion is found in native BPU suggests that this is a potential site for anion binding, stabilized by H-bonds with Arg$^{\alpha 339}$ and His$^{\alpha 323}$, residues thought to be involved in enzyme catalysis. This feature is another important hint for structure-based molecular design.

A comparison of the structures of AHA-inhibited BPU and KAU reveals important features (see Fig. 5A and C). First of all, in both structures the inhibitor bridges and chelates the two Ni ions. However, in KAU the bridging oxygen atom of AHA is asymmetrically bound to Ni(1) (2.6 Å) and Ni(2) (1.8 Å), while the structure of AHA bound to BPU features a symmetric bridge (Ni-O$_B$ distance of 2.0 Å). The latter observation is consistent with the structures of low molecular weight compounds reproducing the binding of AHA to

the dinuclear Ni center of BPU [34, 35]. In all these synthetic models the AHA molecule chelates and symmetrically bridges the two Ni ions with geometrical parameters essentially identical to AHA-inhibited BPU, in slight contrast to the structure of AHA-bound KAU. The high accuracy of the present structure of AHA-complexed BPU, and the good quality of the electron density map around the Ni ions, allow us to unambiguously determine the position of the inhibitor in the active site. Furthermore, the KAU structure is actually that of the recombinant $Cys^{\alpha 322}Ala$ mutant urease (BPU consensus sequence numbering), while the structure of BPU is that of the native enzyme. Finally, the helix-loop-helix motif flanking the active side cavity in the low-temperature structure of AHA-inhibited BPU is in the "open" conformation, while this flap was not detected in the electron density map of AHA-inhibited KAU, probably because of higher disorder at room temperature. However, the conformation of $Ala^{\alpha 363}$ (corresponding to $Ala^{\alpha 366}$ in BPU, see Fig. 5C), shown to be an indicator of the flap position in BPU [10], suggests that the flap preferentially adopts a closed conformation in AHA-inhibited KAU. Such a conformation of $Ala^{\alpha 363}$ in the AHA-KAU adduct allows the formation of an additional H-bond between the carbonyl group of this residue and the AHA NH group, this H-bond possibly being the cause of the asymmetric bridge observed in AHA-inhibited KAU. The importance of the conformation of this flap in the catalytic enzyme mechanism [9, 10] indicates that it is an important determinant for inhibitor binding to the active site.

$$E + I \underset{k_2}{\overset{k_1}{\rightleftharpoons}} E\text{-}I \underset{k_4}{\overset{k_3}{\rightleftharpoons}} E\text{-}I^*$$

$$K_i = \frac{k_2}{k_1}; \quad K_i^* = K_i \bullet \frac{k_4}{k_3 + k_4}$$

Scheme 3

Kinetic studies have shown that AHA is a slow-binding, competitive inhibitor for microbial urease (KAU) [19]: AHA rapidly forms an initial weak enzyme-inhibitor complex (E-I) which slowly converts to a more stable E-I* adduct with an overall dissociation equilibrium constant $K_i^* = 2.6\ \mu M$ (Scheme 3) [19].

Both K_i and k_3 are nearly unchanged in the pH range 6.75–8.25, in the vicinity of the pK_a of AHA (8.7), while k_4 increases by lowering the pH down to 6.5, causing an overall increase of K_i^* [19]. This result suggested to the authors that both the initial E-I complex, as well as the E-I to E-I* conversion, do not involve the acetohydroxamate anion. A mechanism for the formation of the E-I complex was then proposed, by which the resonance form B of AHA (see Scheme 1) is bound in a monodentate mode through the anionic O atom to one Ni ion in the active site [19]. The conversion from E-I to E-I* was proposed to involve either (1) the action of a nucleophile, suggested to be a Ni-bound hydroxide, needed for the formation of a tetrahedral AHA-derived *gem*-diolate, which would bridge the two Ni ions in the dead-end complex, or (2) a bi-

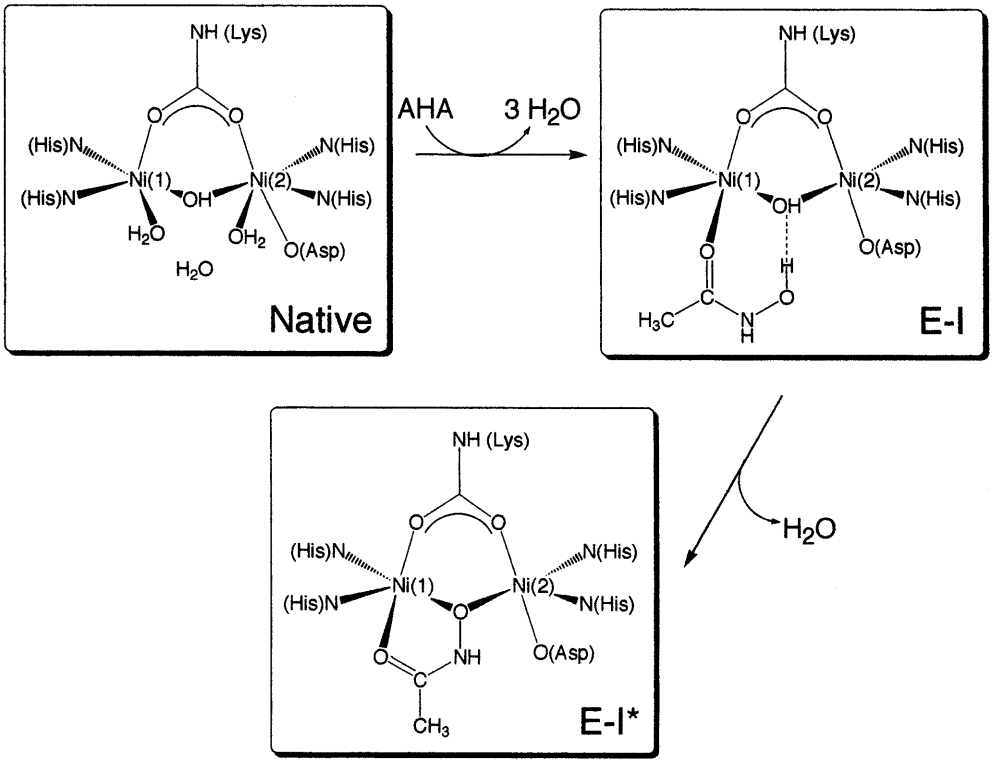

Fig. 6 Proposed mechanism for inhibition of BPU by AHA

dentate binding mode of AHA to the metallocenter [19].

The present structure of AHA-inhibited BPU, assumed to show the E-I* form of the complex because of the long time (days) needed for protein crystallization, rules out the first of the two mechanisms previously proposed, while supporting the second hypothesis. Furthermore, the structure is consistent with the presence of an anionic form of the inhibitor bound to the Ni ions, while showing the absence of the bridging hydroxide. A putative mechanism that could explain both the kinetic and structural evidence is shown in Fig. 6. According to this proposal, an initial E-I complex rapidly forms when the neutral AHA enters the active site and displaces W_1, W_2, and W_3, making a coordination bond between Ni(1) and the carbonyl oxygen of AHA (and possibly also forming an H-bond donated to the bridging hydroxide by the AHA-OH group). A second, slower step would involve the substitution of a Ni-bridging water molecule (possibly formed following proton transfer from the AHA OH group to the bridging hydroxide) by the newly formed hydroxamate oxygen atom, thereby leading to the tight E-I* complex observed crystallographically. This mechanism would be facilitated if the pK_a of AHA in the E-I form of the complex is close to, or smaller than, the pK_a of the bridging water molecule. The pK_a of AHA in the E-I form could be significantly decreased from its value of 8.7 in water by the Ni-induced stabilization of the resonance form B of AHA (see Scheme 1), which places a formal positive charge on the nearby NH group. Further studies are in progress to test the feasibility of this mechanism using docking calculations of AHA to native BPU.

The structures of BPU complexed with cysteamine and phosphate, currently under investigation in our laboratories, will provide further information on the catalytic and inhibition mechanisms of urease.

Acknowledgements We thank the European Union for support of the work at EMBL Hamburg through the HCMP Access to Large Installations Project, contract number CHGE-CT93-0040. S.C. and S.M. acknowledge funding by MURST, Progetti di Interesse Nazionale (ex-40% 1997). S.B. thanks the EMBL for a predoctoral fellowship.

References

1. Mobley HLT, Hausinger RP (1989) Microbiol Rev 53:85–108
2. Collins CM, D'Orazio SEF (1993) Mol Microbiol 9:907–913
3. Mobley HLT, Island MD, Hausinger RP (1995) Microbiol Rev 59:451–480
4. Bremner JM, Krogmeier MJ (1989) Proc Natl Acad Sci USA 86:8185–8188
5. Bremner JM (1995) Fert Res 42:321–329
6. Griffith DP (1978) Kidney Int 13:372–382
7. Sim E, Jones A, Stanley L (1985) Acta Pharmacol Toxicol 57:304–306
8. Krogmeier MJ, McCarty GW, Bremner JM (1989) Proc Natl Acad Sci USA 86:1110–1112
9. Ciurli S, Benini S, Rypniewski WR, Wilson KS, Miletti S, Mangani S (1999) Coord Chem Rev 190–192:331–355
10. Benini S, Rypniewski WR, Wilson KS, Miletti S, Ciurli S, Mangani S (1999) Structure 7:205–216
11. Benini S, Rypniewski WR, Wilson KS, Ciurli S, Mangani S (1998) JBIC 3:268–273
12. Benini S, Ciurli S, Nolting HF, Mangani S (1996) Eur J Biochem 239:61–66
13. Andrews RK, Dexter A, Blakeley RL, Zerner B (1986) J Am Chem Soc 108:7124–7125
14. Kobashi K, Hase J-I, Uehara K (1962) Biochim Biophys Acta 62:380–383
15. Dixon NE, Gazzola C, Watters JJ, Blakeley R, Zerner B (1975) J Am Chem Soc 97:4130–4131
16. Dixon NE, Hinds JA, Fihelly AK, Gazzola C, Winzor DJ, Blakeley RL, Zerner B (1980) Can J Biochem 58:1323–1334
17. Pugh KB, Waid JS (1969) Soil Biol Biochem 1:195–206
18. Clark PA, Wilcox DE (1989) Inorg Chem 28:1326–1333
19. Todd MJ, Hausinger RP (1989) J Biol Chem 264:15835–15842
20. Pearson MA, Overbye ML, Hausinger RP, Karplus PA (1997) Biochemistry 36:8164–8172
21. Benini S, Gessa C, Ciurli S (1996) Soil Biol Biochem 28:819–821
22. Otwinowski Z, Minor W (1997) Methods Enzymol 276:307–325
23. Dauter Z (1997) Methods Enzymol 276:326–344
24. Jones TA, Zou JY, Cowan SW, Kjeldgaard M (1991) Acta Crystallogr Sect A 47:110–119
25. Murshudov GN, Vagin AA, Dodson EJ (1997) Acta Crystallogr Sect D 53:240–255
26. Engh RA, Huber R (1991) Acta Crystallogr Sect A 47:392–400
27. Lamzin VS, Wilson KS (1997) Methods Enzymol 277:269–305
28. Murshudov GN, Vagin AA, Lebedev A, Wilson KS, Dodson EJ (1999) Acta Crystallogr Sect D 55:247–255
29. Vriend G (1990) J Mol Graphics 8:52–56
30. Laskowski RA, MacArthur MW, Moss DS, Thornton JM (1993) J Appl Crystallogr 26:283–291
31. Karplus PA, Pearson MA, Hausinger RP (1997) Acc Chem Res 30:330–337
32. Jabri E, Carr MB, Hausinger RP, Karplus PA (1995) Science 268:998–1004
33. Addison AW, Rao TN, Reedijk J, van Rijn J, Verschoor GC (1984) J Chem Soc Dalton Trans 1349–1356
34. Stemmler AJ, Kampf JW, Kirk ML, Pecoraro VL (1995) J Am Chem Soc 117:6368–6369
35. Arnold M, Brown DA, Deeg O, Errington W, Haase W, Herlihy K, Kemp TJ, Nimir H, Werner R (1998) Inorg Chem 37:2920–2925